Fulde-Ferrell-Larkin-Ovchinnikov vortex lattice states in fermionic cold-atom systems

Y.-P. Shim,[1] R. A. Duine,[1,2] and A. H. MacDonald[1]

[1]*Department of Physics, University of Texas at Austin, Austin, Texas 78712, USA*

[2]*Institute for Theoretical Physics, Utrecht University, Leuvenlaan 4, 3584 CE Utrecht, The Netherlands*

Condensation of atom pairs with finite total momentum is expected in a portion of the phase diagram of a two-component fermionic cold-atom system. This unusual condensate can be identified by detecting the exotic higher-Landau-level (HLL) vortex lattice states it can form when rotated. With this motivation, we have solved the linearized gap equations of a polarized cold-atom system in a Landau-level basis to predict experimental circumstances under which HLL vortex lattice states occur.

I. INTRODUCTION

Polarized two-component fermion systems tend toward finite-pair-momentum condensates because of the Fermi radius mismatch between majority and minority components. In superconductors, electron spin polarization can be induced by the application of an external field or by proximity coupling to a ferromagnet. Finite-momentum Cooper pair condensates in spin-polarized superconductors, Fulde-Ferrell-Larkin-Ovchinnikov (FFLO) states, were first proposed in the early 1960s [1,2]. One important consequence of finite-momentum pairing in an isolated superconductor is a spatially inhomogeneous order parameter. There have been many efforts in various solid-state systems to detect this exotic state, including recent ones [3,4], but its definitive identification has remained elusive. The disorder that is inevitably present in a solid-state system may have played a role in the absence of a conclusive FFLO-state identification in studies of spin-polarized superconductors.

Experimental progress [5–8] with fermionic cold-atom systems has given rise to a strategy for realizing the FFLO state or the related Sarma state [9] and has stimulated a great deal of theoretical activity [10–24]. The tunability of the interaction between atoms via a Feshbach resonance [25,26] has made it possible to increase the strength of fermion pairing and has even made the BEC-BCS crossover [27–29] experimentally accessible. On the Bose-Einstein condensate (BEC) side of a Feshbach resonance fermionic atoms form bosonic molecules which condense at low temperatures. On the Bardeen-Cooper-Schrieffer (BCS) side, the effective attractive interaction between fermion atoms leads to BCS-type pairing. In between lies the so-called unitary limit [30] in which no weakly interacting particle description applies.

Easy control over the population of two hyperfine states in a trapped-atom cloud makes cold-atom systems a promising candidate for FFLO-state realization. The FFLO state competes [10–24] with a number of other states, including in cold-atom systems states with phase-separated regions that are respectively unpolarized and unpaired. The FFLO state is expected to occur on the BCS side of the BEC-BCS crossover, at temperatures and pressures close to the normal-superfluid phase boundary. Population imbalance in cold atoms plays essentially the same role as a Zeeman or exchange field in a superconductors since pairing is dependent on en-

ergy measured from the Fermi energy for each species of fermion. In both cases the Fermi radius of the majority species exceeds the Fermi radius of the minority species and pairs at the Fermi energy necessarily have nonzero total momentum.

One of the most obvious signatures of superfluidity in fermionic cold-atom systems is the appearance of vortices and vortex lattices when the system is rotated [31]. Indeed recent experiments [5] have observed vortex lattice structures in fermionic cold-atom systems close to the BEC-BCS crossover region. For this reason an obvious potential signature of an FFLO state is the appearance of the exotic vortex lattice structures they are expected to form [32–34]. FFLO vortex lattices can be wildly different from the usual hexagonal Abrikosov vortex lattice. The structure of the vortex lattice is determined mainly [32–34] by the Landau-level index of its condensed fermion pairs; the Abrikosov lattice forms when the Landau level index $j=0$, which is the closest approximation to zero-total-momentum pairing allowed in a system that has come to equilibrium in a rotating frame. FFLO states in the absence of rotation can imply $j>0$ fermion pair condensation in rotated systems. Vortices have been observed in systems with population imbalance [6], but so far no unusual vortex structures have been observed. (This could be due to the fact that these experiments realize the gapless Sarma phase [24], and another reason could be that the FFLO state is predicted by weak-coupling theory while all experiments are in the unitary limit.)

With this motivation, we report on a study of the polarization and interaction strength regime over which nonzero j pairing is expected in a rotating two-component fermion system. We consider only the BCS side of the Feshbach resonance on which FFLO physics occurs. We consider three-dimensional systems for the sake of definiteness, although two-dimensional systems could also be interesting experimentally. Working in the corotating reference frame, rotation is equivalent to an external magnetic field and a reduction in radial confinement strength. All our explicit calculations are for a uniform three-dimensional system and do not account for confinement. In typical experiments the atomic Landau-level splitting, equal to $2\hbar\Omega$ where Ω is the rotation frequency, is much smaller than the Fermi energy. In this limit the Landau-level index of the condensate could be determined by finding the optimal pairing wave vector on the BCS superfluid-normal phase boundary in the absence of

$$k_{F\uparrow} = k_{F\downarrow}, \quad Q = 0 \qquad\qquad k_{F\uparrow} \neq k_{F\downarrow}, \quad Q = k_{F\uparrow} - k_{F\downarrow}$$
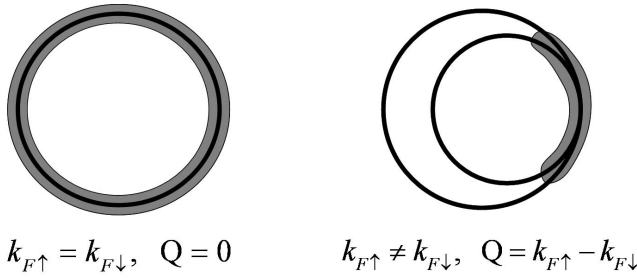
FIG. 1. Low-energy pairings for population-balanced and population-unbalanced systems. Shaded regions indicate participating states for the low-energy parings in k space. Q is the total momentum of the pairs, which is 0 for balanced systems and equal to the difference between Fermi wave vectors in unbalanced systems.

rotation and using semiclassical quantization to add rotation to the condensate effective action. Here we use a fully quantum-mechanical approach, including Landau quantization even at the level of the underlying unpaired fermions. This approach is still relatively easy, partly because of the short range of the atom-atom attractive effective interaction and has the advantage of determining the condensate Landau-level index more accurately and allows us to comment on the rapid rotation regime which might be approached experimentally in the future. From now on we use the language of the corotating frame so that the atoms experience an effective field with cyclotron frequency $\Omega_c = 2\,\Omega$.

Pairing is most effective when the states to be paired are as close to the Fermi energy as possible. When there is no population imbalance, pairs formed from electrons with opposite momentum (zero total momentum) are abundant at low energies as illustrated schematically in Fig. 1. For unbalanced populations the lowest-energy pairs have total momentum equal to the difference between Fermi wave vectors. In systems with an orbital magnetic field linear momentum is not a good quantum number, but the motion of a pair can still be separated into center-of-mass and relative motion degrees of freedom. In a magnetic field, momentum space collapses into Landau levels whose degeneracy is illustrated in Fig. 2 by partitioning of momentum space into equal-area segments centered on $\hbar\Omega_c(N+1/2)$. A pair of electrons with given Landau-level indices N and N' has finite quantum amplitudes for all center-of-mass Landau-level indices from 0 to $N+N'$ which correspond closely to the distribution of center-of-mass (c.m.) kinetic energy values that would be obtained by averaging over the corresponding regions of momentum space illustrated in Fig. 2. These quantum probability amplitudes are the key ingredient in the linearized gap equations discussed below. We derive linearized gap equations which implicitly define the critical temperature for a phase transition from the normal to the superfluid state for each c.m. LL and determine the phase boundaries in parameter space. If excited c.m. LL's have a higher critical temperature than the lowest-lying c.m. LL, this signals the occurrence of exotic vortex lattice states and of FFLO states in the unrotated system. In Fig. 3 the phase diagram is shown for a nonrotating homogeneous system. The maximum value of the exchange field (or difference between normal-state chemical poten-
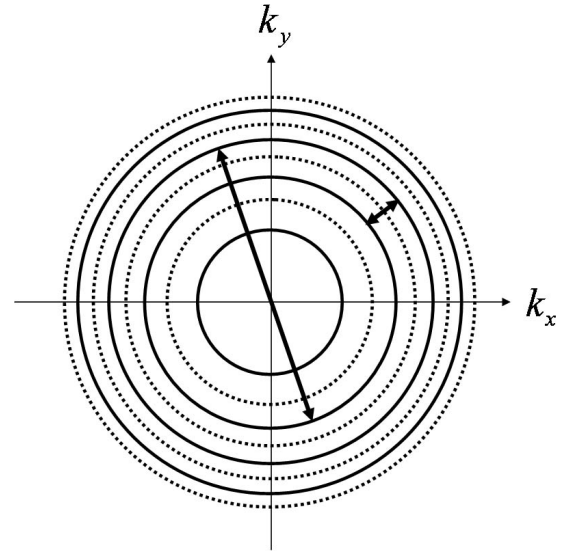

FIG. 2. Degeneracy of Landau levels. States between two dotted circles collapse into the solid circle. All the areas between two adjacent dotted circles are the same, and solid circles have radii given by $\hbar^2 k^2/2m = \hbar\Omega_c(N+1/2)$. The arrows show the maximum and minimum momentum differences between particles in LL $N=1$ and $N=2$, which correspond qualitatively to the maximum and minimum of the c.m. momentum.

tials) for which pairing still occurs is given approximately by $H = \Delta_0/\sqrt{2}$, where Δ_0 is the BCS gap parameter at zero exchange field and zero temperature. Beyond this so-called Clogston limit [36] the BCS state is no longer stable. The FFLO state is expected to occur in this region of the phase diagram.

The rest of the paper is organized as follows. In Sec. II we derive c.m. Landau-level-index-dependent linearized gap equations for the critical temperature of the rotating system. The numerical solution of this equation is presented in Sec.
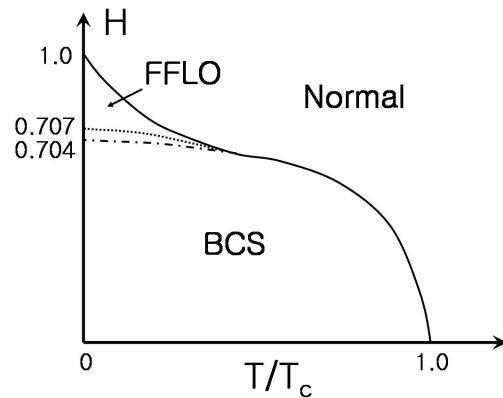

FIG. 3. BCS theory phase diagram for FFLO and BCS states as calculated, for example, in Ref. [35]. Here, H is the ratio of the Zeeman energy (or normal-state chemical potential difference) to the zero-field energy gap. The dotted line marks the Clogston limit where the energies of normal and zero-pairing-momentum BCS states are identical. The FFLO state occurs near the boundary between normal and BCS states.

III. We finish in Sec. IV with a discussion of our results and present our conclusions. We postpone to this section a discussion of the competition between phase-separated states and FFLO states, which is an issue for cold atoms but not for electrons in a solid because of long-range repulsive Coulomb interactions.

II. LINEARIZED GAP EQUATIONS

In this section we derive the linearized gap equation for condensation of Fermion pairs with a definite c.m. Landau-level (LL) index. We first consider the transformation between individual particle and c.m. and relative states for two rotating atoms and then use this to derive the gap equations, which are implicit equations for the critical temperatures of each c.m. LL index channel.

A. Unitary transformation

To consider the pairing instability of a normal Fermi gas, we first turn our attention to the description of scattering between two atoms in a rotating reference frame. The rotation is represented by considering the atoms to be particles with unit charge in an effective homogeneous orbital magnetic field. The Hamiltonian for two particles is

$$\hat{h} = \frac{1}{2m}[-i\hbar\boldsymbol{\nabla}_{\mathbf{r}_1} - \mathbf{A}(\mathbf{r}_1)]^2 + \frac{1}{2m}[-i\hbar\boldsymbol{\nabla}_{\mathbf{r}_2} - \mathbf{A}(\mathbf{r}_2)]^2$$
$$= \frac{1}{2M}[-i\hbar\boldsymbol{\nabla}_{\mathbf{R}} - 2\mathbf{A}(\mathbf{R})]^2 + \frac{1}{2\mu}\left(-i\hbar\boldsymbol{\nabla}_{\mathbf{r}} - \frac{\mathbf{A}(\mathbf{r})}{2}\right)^2, \quad (1)$$

where $M=2m, \mu=m/2$, $\mathbf{R}=(\mathbf{r}_1+\mathbf{r}_2)/2$, and $\mathbf{r}=\mathbf{r}_1-\mathbf{r}_2$. The vector potential $\mathbf{A}(\mathbf{r})$ is defined by $\boldsymbol{\nabla}\times\mathbf{A}(\mathbf{r})=2m\Omega\hat{\mathbf{z}}$ where Ω is the angular rotation frequency of the system, and we assume that the rotation is around the z axis. In the Landau gauge, $\mathbf{A}(\mathbf{r})=(0,2m\Omega x,0)$ and the individual atom eigenfunctions with eigenvalues $\hbar\Omega(2N+1)$ are given by

$$\psi_{N,k_{i,y},k_{i,z}}(\mathbf{r}_i) = \langle\mathbf{r}_i|N,k_{i,y},k_{i,z}\rangle$$
$$= e^{i(k_{i,y}y_i+k_{i,z}z_i)}\phi_N(x_i+k_{i,y}l_B^2)/(L_yL_z)^{1/2}, \quad (2)$$

where $\phi_N(\mathbf{r})$ is the one-dimensional harmonic oscillator eigenfunction and the effective magnetic length l_B is defined by $\hbar^2/ml_B^2=2\hbar\Omega$. The eigenfunctions are labeled by the momenta in the y and z directions and by the LL index N. The eigenfunctions for the c.m. and relative coordinates are the same, except that the effective magnetic lengths are now $l_R=l_B/\sqrt{2}$ and $l_r=\sqrt{2}l_B$. In terms of ladder operators,

$$\hat{h} = \hbar\Omega_c(a_1^\dagger a_1 + a_2^\dagger a_2 + 1) = \hbar\Omega_c(a_R^\dagger a_R + a_r^\dagger a_r + 1), \quad (3)$$

where $a_i=(l_B/\sqrt{2}\hbar)(\pi_{i,x}-i\pi_{i,y})$, $\boldsymbol{\pi}_i=i\hbar\boldsymbol{\nabla}_i-\mathbf{A}(\mathbf{r}_i)$, $a_R=(a_1+a_2)/\sqrt{2}$, $a_r=(a_1-a_2)/\sqrt{2}$, and $\hbar\Omega_c=\hbar^2/ml_B^2=2\hbar\Omega$. The ladder operators can then be used to derive [37] an explicit expression for the unitary transformation between individual particle and c.m. and relative two-atom states:
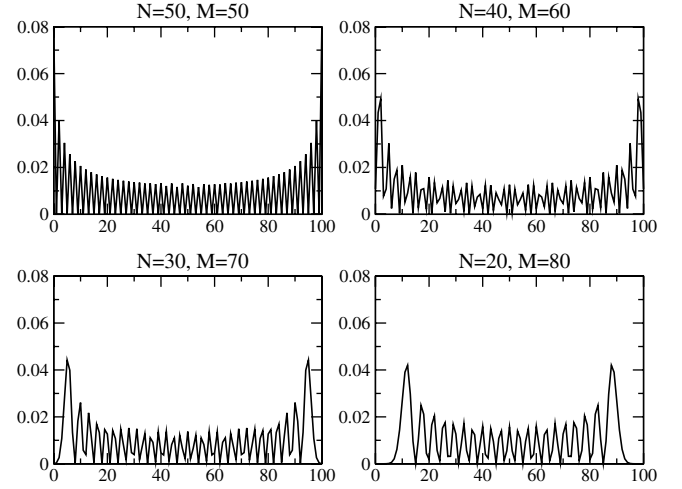

FIG. 4. $|B_j^{NM}|^2$ vs j with $N+M=100$ for different N's. The horizontal axes are j and the vertical axes are $|B_j^{NM}|^2$.

$$\langle\mathbf{r}_1,\mathbf{r}_2|N,k_{1,y},k_{1,z};M,k_{2,y},k_{2,z}\rangle$$
$$= \sum_{j=0}^{N+M} B_j^{NM}\langle\mathbf{R},\mathbf{r}|j,K_y,K_z;N+M-j,k_y,k_z\rangle, \quad (4)$$

where

$$K_y = k_{1,y}+k_{2,y}, \quad K_z = k_{1,z}+k_{2,z},$$
$$k_y = (k_{1,y}-k_{2,y})/2, \quad k_z = (k_{1,z}-k_{2,z})/2,$$

and

$$B_j^{NM} = \left[\frac{j!(N+M-j)!N!M!}{2^{N+M}}\right]^{1/2}$$
$$\times \sum_{m=0}^{j} \frac{(-1)^{M-m}}{(j-m)!(N+m-j)!(M-m)!m!}. \quad (5)$$

It follows that B_j^{NM} is the probability amplitude for two atoms in LL's N and M, respectively, to have c.m. LL j and the relative motion LL $N+M-j$. When $N=M$, $|B_j^{NM}|^2$ has maxima for $j=0$ and $j=N+M$. However, if $N\neq M$, $|B_j^{NM}|^2$ can have a maximum for intermediate j, which means that for two atoms in different LL's, the most probable c.m. LL can be different from zero or $N+M$ as shown in Fig. 4. The smooth envelope apparent in these figures is simply the zero-field probability distribution of the c.m. kinetic energies given the Fermi momenta of two individual particles. The c.m. energy is maximum for parallel momentum and minimum for oppositely oriented individual particle momenta. This coefficient plays an important role in determining the pairing c.m. LL in condensed states.

B. Bethe-Salpeter equations

The pairing instability in a Fermi gas is signaled by a divergence of the many-body scattering function [38], which we approximate using the Bethe-Salpeter equation summarized by the finite-temperature Feynman diagrams illustrated
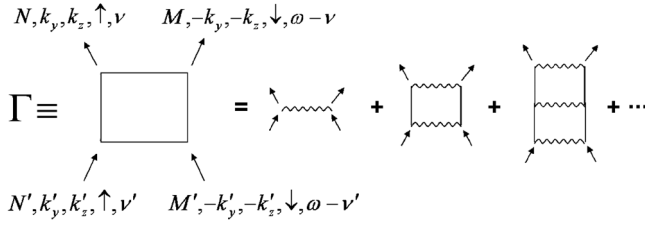
FIG. 5. Ladder diagrams to be summed for scattering function Γ.

in Fig. 5. We consider a system consisting of two hyperfine species denoted by $\uparrow$ and $\downarrow$. For definiteness we assume that the two species have the same energy spectrum but allow for different densities and therefore different chemical potentials. Population imbalance is relatively easy to achieve experimentally and the lifetime of each hyperfine state is long enough compared to experimental time scales to justify the use of equilibrium statistical mechanics with separate particle reservoirs for the two species. The many-body scattering function is calculated by summing the ladder diagrams [37,39] (see Fig. 5). Generalizing the calculations of Ref. [37] to three dimensions from two and we find that the total two-particle scattering function can be written as a sum over different c.m. Landau-level index channels:

$$\Gamma(N,M,k_y,k_z;N',M',k'_y,k'_z;i\omega)$$
$$= \sum_j B_j^{NM} B_j^{N'M'} \gamma_j(N,M,k_y,k_z,N',M',k'_y,k'_z;i\omega), \quad (6)$$

where the partial scattering function for c.m. LL j,

$$\gamma_j(N,M,k_y,k_z;N',M',k'_y,k'_z;i\omega)$$
$$= \langle N+M-j,k_y,k_z|\hat{V}|N'+M'-j,k'_y,k'_z\rangle$$
$$+ \sum_{N'',M''} \sum_{k''_y,k''_z} |B_j^{N''M''}|^2$$
$$\times \langle N+M-j,k_y,k_z|\hat{V}|N''+M''-j,k''_y,k''_z\rangle$$
$$\times K_{N'',M'',k''_z}(i\omega) \gamma_j(N'',M'',k''_y,k''_z;N',M',k'_y,k'_z.\;;i\omega). \quad (7)$$

In Eq. (7),

$$K_{N,M,k_z}(i\omega) = \frac{1 - f(\xi_{N,k_z,\uparrow}) - f(\xi_{M,-k_z,\downarrow})}{i\hbar\omega - \xi_{N,k_z,\uparrow} - \xi_{M,-k_z,\downarrow}}, \quad (8)$$

$$\xi_{N,k_z,\sigma} = \varepsilon_{N,k_z} - \mu_\sigma, \quad (9)$$

$$\varepsilon_{N,k_z} = \hbar\Omega_c\left(N + \frac{1}{2}\right) + \frac{\hbar^2 k_z^2}{2m}, \quad (10)$$

and $f(\xi)$ is the Fermi distribution function. In the case of a δ-function interaction $V(\mathbf{r}) = -V_0\delta(\mathbf{r})$ we have that

$$\langle N+M-j,k_y,k_z|\hat{V}|N'+M'-j,k'_y,k'_z\rangle$$
$$= -V_0\phi^r_{N+M-j}(k_y l_r^2)\phi^r_{N'+M'-j}(k'_y l_r^2)(1/L_y L_z), \quad (11)$$

where ϕ^r_N is the one-dimensional harmonic oscillator eigenfunction in relative coordinates. Using this property and the orthogonality of the relative motion harmonic oscillator wave functions we find that

$$\gamma_j(N,M,k_y,k_z;N',M',k'_y,k'_z;i\omega)$$
$$= \frac{-V_0}{L_y L_z}\phi^r_{N+M-j}(k_y l_r^2)\phi^r_{N'+M'-j}(k'_y l_r^2)$$
$$\times \left(1 + \frac{V_0}{4\pi l_B^2 L_z}\sum_{N'',M'',k''_z} K_{N'',M'',k''_z}(i\omega)|B_j^{N''M''}|^2\right)^{-1}. \quad (12)$$

C. T_c equation

As mentioned before, the instability of the normal state due to pairing is signaled by the divergence of the many-body scattering function $\Gamma(i\omega=0)$, and therefore a diverging $\gamma_j(i\omega=0)$ means that pairs with c.m. LL j are unstable to condensation. This instability condition for the scattering function is equivalent to the linearized gap equation which defines the critical temperature [38] in mean-field theory. (In mean-field-theory for the ordered state [40] the order parameter can be expressed in terms of partial contributions from each c.m. LL channel. When the order parameter is small the various channels decouple and the partial contribution from a given channel vanishes at the same point at which the normal-state partial scattering function diverges.) From Eq. (12), we get an implicit equation for the critical temperature T_c^j for each c.m. LL j, which reads

$$\frac{1}{V_0} = \frac{1}{4\pi l_B^2 L_z}\sum_{N,M,k_z}\frac{1 - f(\xi_{N,k_z,\uparrow}) - f(\xi_{M,-k_z,\downarrow})}{\xi_{N,k_z,\uparrow} + \xi_{M,-k_z,\downarrow}}|B_j^{NM}|^2. \quad (13)$$

Unlike the BCS superconductors, for which retarded phonon-mediated attractive interactions have a natural ultraviolet cutoff, there is no cutoff in this equation and the summation is over all states. Hence, as it stands, this equation diverges, because of the assumption of a δ-function interaction. To remove this divergence, we need to recognize that the true atom-atom interaction is short ranged compared to relevant atomic wavelengths but not a δ function. Using the exact relation between scattering length and interaction strength [see Eq. (A5) in the Appendix] we remove the interaction strength V_0 by renormalizing to the scattering length [39] in the T_c^j equation and obtain convergent sums over intermediate states. The equation for T_c^j then becomes

$$-\frac{1}{k_{F0}a_{\text{sc}}} = \frac{\hbar\Omega_c}{2\pi k_{F0}} \sum_{N,M} \int dk_z \left[\frac{1 - f(\xi_{N,k_z,\uparrow}) - f(\xi_{M,-k_z,\downarrow})}{\xi_{N,k_z,\uparrow} + \xi_{M,-k_z,\downarrow}} |B_j^{NM}|^2 \right.$$

$$\left. - \frac{1}{\varepsilon_{N,k_z} + \varepsilon_{M,-k_z}} |B_0^{NM}|^2 \right], \tag{14}$$

where k_{F0} is the Fermi wave vector of the unpolarized system without rotation. The left-hand side of Eq. (14) is experimentally measurable. We determine T_c as a function of $1/k_{F0}a_{\text{sc}}$ by solving this implicit equation combined with implicit equations for the temperature-dependent chemical potentials μ_σ:

$$n_\sigma = \frac{1}{V} \sum_{N,k_y,k_z} f(\varepsilon_{N,k_z} - \mu_\sigma), \tag{15}$$

where n_σ is the density of atoms in hyperfine state σ and V is the total volume of the system. In the next section we present numerical results obtained by solving these equations.

III. NUMERICAL RESULTS

We calculate T_c^j for each c.m. LL j for various rotation frequencies, interaction strengths, and polarizations and in this way determine the phase boundaries in the parameter space spanned by $\hbar\Omega_c$, a_{sc}, and the polarization. We fix the total density of the system, n_{tot}, and use the polarization p as a parameter. The polarization is defined by

$$p = \frac{n_\uparrow - n_\downarrow}{n_\uparrow + n_\downarrow}, \tag{16}$$

where $n_\uparrow$ is the density of the majority species and $n_\downarrow$ is the density of the minority species. Hence, the density of atoms in species σ [$\sigma = +1 \ (-1)$ corresponds to $\uparrow \ (\downarrow)$] is given by

$$n_\sigma = \frac{1 + \sigma p}{2} n_{\text{tot}}. \tag{17}$$

The relationship between T_c^j and interaction strength is illustrated in Fig. 6. The true critical temperature for the system is the largest value of T_c^j:

$$T_c = \max\{T_c^j\}. \tag{18}$$

At weak rotation [Fig. 6(a)], the transition temperature T_c for zero polarization shows the usual behavior [41] $T_c \propto \exp(-1/k_{F0}a_{\text{sc}})$ and the highest T_c^j is for the $j=0$ channel regardless of the interaction strength. In this circumstance we expect the system will have a standard Abrikosov vortex lattice. The critical temperature decreases as polarization increases and superfluidity is suppressed above some critical polarization. It is more easily suppressed at weak interaction. FFLO states, which correspond to nonzero j, occur at strong
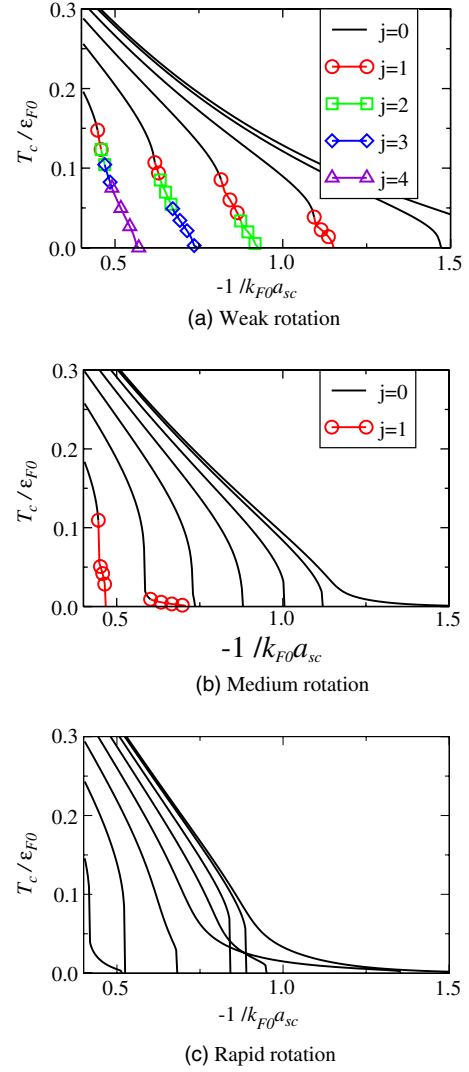

(a) Weak rotation

(b) Medium rotation

(c) Rapid rotation

FIG. 6. (Color online) Critical T_c vs $-1/k_{F0}a_{\text{sc}}$. (a) $\hbar\Omega_c/\varepsilon_{F0}=0.02$. The curves are for different polarizations 0.0, 0.1, 0.2, 0.3, 0.4, 0.5 from top to bottom. (b) $\hbar\Omega_c/\varepsilon_{F0}=0.17$. Polarizations are from 0.0 to 0.6. (c) $\hbar\Omega_c/\varepsilon_{F0}=0.50$. Polarizations are from 0.0 to 0.7.

interaction and high polarization. We emphasize that these states will have very distinct [34] vortex lattices, more open than the hexagonal Abrikosov lattices and qualitatively different for each value of j. It should be quite obvious experimentally when a $j \neq 0$ vortex lattice occurs. We caution, however, that as the temperature drops below the critical temperature, different values of j will mix in the condensate [37,40] and the $j=0$ component will grow in weight even if it does not have the maximum T_c. We speculate that the phase transition between finite-momentum FFLO states and zero-momentum BCS states, which occurs at zero field, is replaced in the field by a smooth crossover between open and close-packed hexagonal lattices. The best place to search experimentally for an exotic vortex lattice is close to the superfluid-normal phase boundary as possible by varying either temperature or interaction strength. Indeed it appears

advisable to conduct experiments in systems with the smallest order parameter strength for which it is possible to reliably visualize the vortex lattice. Both the relatively large polarizations and strong interactions required for the appearance of $j \neq 0$ solutions and the ability to tune parameters over wide ranges in atomic systems demonstrate the exceptional potential of tunable cold-atom systems in the hunt for FFLO vortex latices. The greatest obstacle to realization of the FFLO state is likely competition with phase-separated states. We return to this point again later.

The results reported in Fig. 6(a) can be understood qualitatively using quite simple considerations. When the temperature is low, weak pairing is expected to be dominated by states at the Fermi energy. For that reason, the zero-field pairing wave vector on the phase boundary is expected to be close to $k_{F\uparrow} - k_{F\downarrow}$ when $T_c \to 0$—i.e., when the interactions are just strong enough to cause pairing. Using a small-p approximation it follows that the pairing wave vector for $T_c \to 0$ is given approximately by

$$Q = \frac{2k_{F0}p}{3}. \tag{19}$$

The Landau-level index at finite fields can be estimated by quantizing the pairing wave vector. This gives

$$j \approx \frac{(\hbar^2 Q^2)/4m}{\hbar \Omega_c} \simeq \frac{\varepsilon_{F0}}{\hbar \Omega_c} \frac{2p^2}{9}. \tag{20}$$

It is easy to check that this equation is quite consistent with the numerical results we have obtained. For smaller values of $\hbar \Omega_c$ we therefore are confident that even larger values of j should occur, although exotic vortex latices may again be confined even more strongly to the region close to the phase boundary. For a given value of polarization, the value of j decreases with increasing interaction strength because T_c moves to higher temperatures, reemphasizing the importance of pairing precisely at the Fermi energy.

Figures 6(b) and 6(c) show results for systems with larger values of $\hbar \Omega_c$ than have been reported in experiments to date. One observation is that nonzero j states are less likely to occur at large $\hbar \Omega_c$ and appear only at very high polarization and strong interactions. This property is explained by Eq. (20). Indeed one can check that the appearance of nonzero j values is again consistent with this estimate. Other new features that emerge in these figures are due mainly to large LL quantization effects. At very high rotation frequency [Fig. 6(c)], only the $j=0$ c.m. LL is realized. Note that at high temperature, all graphs look similar. (T_c decreases monotonically as the polarization increases and as the interaction strength decreases.) T_c is more weakly dependent on the rotation frequency. This is because the thermal energy is comparable to or larger than the energy quantization due to rotation. On the other hand, at low temperatures, the LL quantization effects become important because the particles have one-dimensional densities of states for each Landau level, leading to peaks in pairing (at least in this
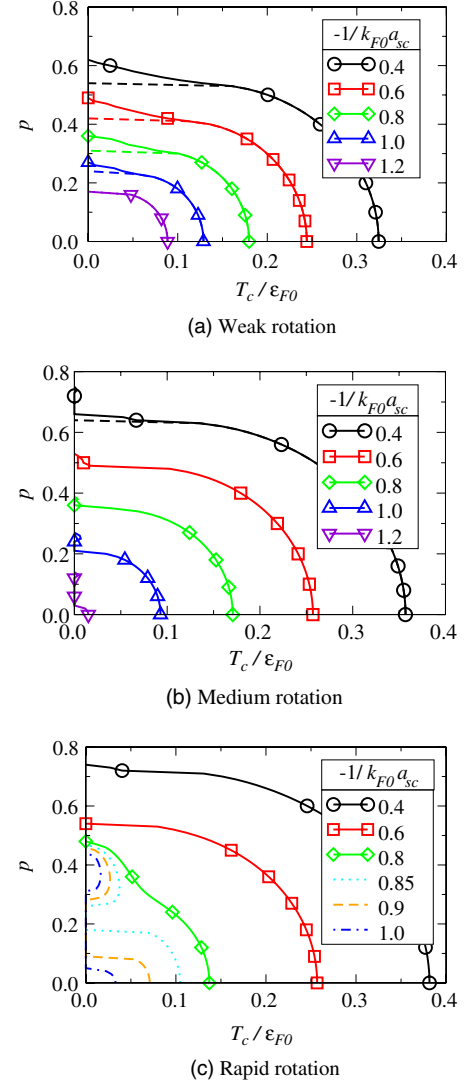

(a) Weak rotation

(b) Medium rotation

(c) Rapid rotation

FIG. 7. (Color online) Polarization vs T_c/ε_{F0}. (a) $\hbar\Omega_c/\varepsilon_{F0}=0.02$. Curves are for different values of $-1/k_{F0}a_{sc}$. (b) is for $\hbar\Omega_c/\varepsilon_{F0}=0.17$ and (c) is for $\hbar\Omega_c/\varepsilon_{F0}=0.50$. Dashed lines in (a) and (b) show the T_c curves for $j=0$ and all the curves in (c) correspond to $j=0$.

mean-field-theory calculation) when any Landau level is just slightly occupied. The nonmonotonic density of states becomes important when the LL spacing is much larger than the temperature. In this case, we expect nonmonotonic behavior that is sensitive to the density of both hyperfine species; we expect nonmonotonic dependence on polarization and the occasional appearance of strong condensates at very large polarizations. Some of this nonmonotonic behavior is evident in Fig. 6(c).

In Fig. 7 we show the phase boundaries versus polarization and temperature for a series of interaction strengths. For slow rotation [Fig. 7(a)] it is similar to the usual BCS-FFLO phase diagram (compare with Fig. 3). At higher rotation frequencies, shown in Fig. 7(b), FFLO states are less likely to occur. The transition temperature still decreases monotonically as the polarization increases, and above some critical polarization, the normal state prevails. At very high rotation
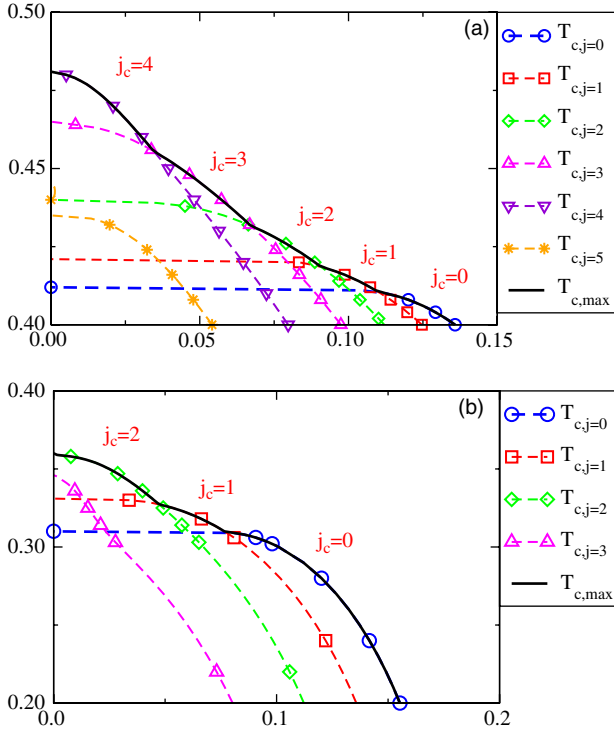
FIG. 8. (Color online) Enlarged figures of Fig. 7(a) for $-1/k_{F0}a_{sc}=$(a) 0.6 and (b) 0.8 near the phase boundaries between FFLO states and normal fluid. The horizontal axis shows T_c/ε_{F0} and the vertical axis is polarization. We calculate T_c for different j's and determine the optimal j that gives the highest T_c.

frequencies, shown in Fig. 7(c), the LL quantization effects become more important and we observe a reemergence of condensed states at around $p=0.4$. The difference of the Fermi energies at this polarization is exactly equal to the LL spacing, and the dominant pairing occurs between individual particles whose Landau-level indices differ by 1.

In Fig. 8 we show an enlargement of the phase diagram for the FFLO state, showing also the critical temperatures for a number of different c.m. LL index channels j in addition to the one with the largest T_c. When the polarization is small, $j=0$ pairing leads to the highest T_c; that is, $j=0$ is the optimal pairing channel for condensation which we denote as j_c. As the polarization increases, T_c^j for nonzero j is larger than $T_c^{j=0}$ and j_c increases with the polarization. This is analogous to having an increasing pairing c.m. momentum with increasing polarization field in the zero-field case. For a given value of $\hbar\Omega_c$, nonzero values of j_c are more likely when interactions are stronger, because the superfluid has to be able to withstand the ill effects of polarization out to a sufficiently large value of p. If the interaction is too weak, no nonzero j pairing can occur and j_c is zero.

In Fig. 9 we plot the phase diagram versus polarization and effective interaction space for slow, intermediate, and rapid rotations. The critical polarization decreases as the interaction strength decreases for weak rotations [Fig. 9(a)], as seen in experiment [6]. The regions labeled FFLO in this figure have $j \neq 0$ condensates at the normal-superfluid boundary. Quite generally this behavior occurs only in a
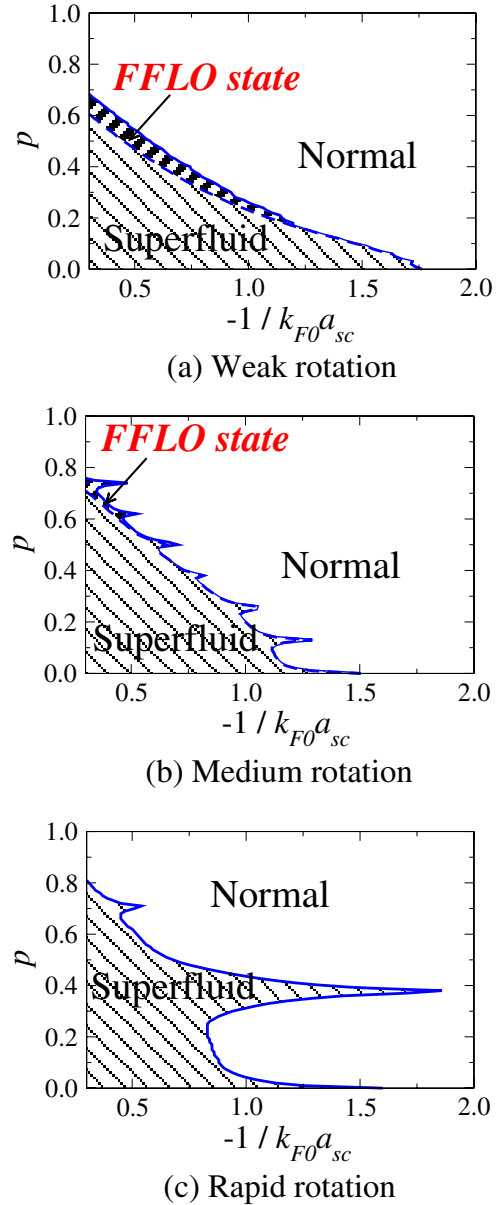

FIG. 9. (Color online) Polarization vs $-1/k_{F0}a_{sc}$. We calculate T_c for polarizations from 0 to 1 with increment 0.01 and choose the largest one that has a finite T_c. (a) $\hbar\Omega_c/\varepsilon_{F0}=0.02$, (b) $\hbar\Omega_c/\varepsilon_{F0}=0.17$, and (c) $\hbar\Omega_c/\varepsilon_{F0}=0.50$. Solid blue curves show the phase boundary between normal fluid and superfluid, and dashed blue curves in (a) and (b) show the phase boundary for c.m. LL $j=0$.

small region along the boundary between the superfluid and normal state in the regime of large polarization and strong interactions. Faster rotation generally suppresses FFLO states, as emphasized earlier, but the superfluid phase can be realized at high polarization and weak interaction by tuning the system such that the Fermi energy mismatch between majority and minority species is an integer times the LL spacing and the Fermi energies are close to a quantized LL energy. In Fig. 9(c), we see that large peaks occur if these conditions are met. At zero polarization, $\varepsilon_{F\uparrow}=\varepsilon_{F\downarrow}=1.96$, in units of LL spacing, and the lowest LL is at 0.5. For

$p=0.41$, $\varepsilon_{F\uparrow}=2.52$ and $\varepsilon_{F\downarrow}=1.52$, so that the Fermi energy difference is exactly the LL spacing and each Fermi energy is very close to the LL's. For $p=0.72$, $\varepsilon_{F\uparrow}=2.80$ and $\varepsilon_{F\downarrow}=0.80$.

IV. DISCUSSION AND CONCLUSIONS

In summary, we have derived an equation for the superfluid critical temperature in rotating fermionic cold-atom systems, incorporating Landau-level quantization effects. Using this equation we have calculated the phase boundary between the normal and superfluid phases considering pairing in different center-of-mass Landau levels. We find that states with higher-Landau-level condensates can occur on the boundary between the normal and superfluid phase regions in a parameter space that can in principle be explored systematically by taking advantage of Feshbach resonances and of the ability to create arbitrary degrees of hyperfine-state polarization in an atom cloud. These FFLO vortex lattice states will have distinct vortex lattices [32–34] which should aid their identification. High polarization and strong interactions are required to realize the FFLO state. At high rotation frequency, features that originate from rotational quantization effects play an important role and we find that for certain parameters the superfluid phase persists to high polarization.

The regime where the FFLO state occurs in rotating systems seems accessible to experiment, and hence we believe that these exotic vortex structures are observable. The greatest obstacle to their observation may be competition with states in which the atoms phase separate into regions with condensation but no polarization and regions with polarization but no condensation. We believe that FFLO physics would almost certainly occur if phase separation could be suppressed. Phase separation does not occur for electrons in a superconducting metal, and cannot because of the large Coulomb energy price that would have to be paid. One possibility for suppressing phase separation in atomic systems with attractive interactions is to artificially create the necessary weak but long-range repulsive interactions by electrically inducing dipoles [42] in a pancake-shaped [43], but not necessarily quasi-two-dimensional trapped-atom system. The typical dipole-dipole interaction energy is $p^2/R^3 \sim p^2 n \sim \alpha^2 E^2 n$ where p is the dipole moment induced by the external electric field E, R is the average interatom distance, n is the density of the atoms, and α is the polarizability of the atom. If this energy is much smaller than the typical atom-atom interaction energy $\varepsilon_{F0}(k_{F0}|a_{sc}|)$, then the physics on short-length scales does not change much. On the other hand, if the energy cost of the whole system due to the long-range dipole interaction when the system is phase separated is much larger than the condensation energy gain, phase separation can be suppressed. Thus, $p^2 n^2 V \gg D(0)\Delta_0^2 \sim N\varepsilon_{F0}e^{-\pi/k_{F0}|a_{sc}|}$ where $D(0)$ is the density of states at the Fermi level, N is the number of atoms, and V is the volume of the system. These conditions lead to a condition for the external electric field,

$$e^{-\pi/k_{F0}|a_{sc}|} \ll \frac{\alpha^2 nE^2}{\varepsilon_{F0}} \ll k_{F0}|a_{sc}|, \tag{21}$$

which can be easily satisfied for small $k_{F0}|a_{sc}|$. FFLO states are most likely expected to occur near the critical temperature T_c while experimentally observed phase-separated states are well below T_c. It is known that phase separation is less likely at higher temperatures, so it could be possible to observe FFLO states near T_c without explicitly suppressing phase separation.

Finally we mention that peculiar additional interesting effects occur because of Landau-level quantization if the rotation frequency is sufficiently large. Very large rotation frequencies have been achieved in experiments with bosonic atoms [44]. We believe, therefore, that there is no fundamental obstacle to approaching the rapid-rotation limit with fermions. Although we have used mean-field theory here to study this regime, there is every reason to expect unanticipated properties to emerge from strong quantum fluctuations and correlations. At sufficiently rapid rotations, it should be possible to for the first time study the fractional quantum Hall effect in fermion systems with attractive interactions [45].

APPENDIX: TWO-BODY TRANSITION MATRIX AND SCATTERING LENGTH IN SYSTEMS WITH ORBITAL MAGNETIC FIELD

In this appendix, we derive the relation between the scattering length and the strength of the δ-function-like particle-particle interaction in a system with orbital magnetic field. The two-body transition operator for scattering at energy z is defined by

$$\hat{T}^{2B}(z) \equiv \hat{V} + \hat{V}\frac{1}{z-\hat{H}_0}\hat{V} + \cdots = \hat{V} + \hat{V}\frac{1}{z-\hat{H}_0}\hat{T}^{2B}(z), \tag{A1}$$

where $\hat{V}$ is the particle-particle interaction and $\hat{H}_0$ is the non-interacting part of the two-body Hamiltonian. The matrix elements of this transition operator satisfy the Lippman-Schwinger equation. Noting that scattering conserves the c.m. motion, we calculate the T-matrix elements in relative-motion Hilbert space with c.m. LL j and c.m. momenta K_y and K_z. Notice that the relative motion T matrix does not depend on the y component of the total momentum K_y in the Landau gauge. In the c.m. and relative coordinate representation we find

$$\langle N + M - j, k_y, k_z | \hat{T}^{2B}(j, K_z; z) | N' + M' - j, k'_y, k'_z \rangle$$

$$= \langle N + M - j, k_y, k_z | \hat{V} | N' + M' - j, k'_y, k'_z \rangle$$

$$+ \sum_{N'', M''} \sum_{k''_y, k''_z} \frac{\langle N + M - j, k_y, k_z | \hat{V} | N'' + M'' - j, k''_y, k''_z \rangle | B_j^{N''M''} |^2 \langle N'' + M'' - j, k''_y, k''_z | \hat{V} | N' + M' - j, k'_y, k'_z \rangle}{z - \varepsilon_{N'', K_z/2 + k''_z} - \varepsilon_{M'', K_z/2 - k''_z}} + \cdots . \quad \text{(A2)}$$

Using Eq. (11) we have that

$$\langle N + M - j, k_y, k_z | \hat{T}^{2B}(j, K_z; z) | N' + M' - j, k'_y, k'_z \rangle$$

$$= \frac{-V_0}{L_y L_z} \phi^r_{N+M-j}(k_y l_r^2) \phi^r_{N'+M'-j}(k'_y l_r^2)$$

$$\times \left[1 - \frac{-V_0}{4\pi l_B^2 L_z} \sum_{N'', M'', k''_z} \frac{|B_j^{N''M''}|^2}{z - \varepsilon_{N'', K_z/2 + k''_z} - \varepsilon_{M'', K_z/2 - k''_z}} \right]^{-1} .$$

$$\text{(A3)}$$

For a dilute atomic gas, all the relevant energies are small compared to $\hbar^2 / m r_V^2$ where r_V is the interaction range. We are therefore allowed to neglect the energy dependence of the two-body T matrix [39]. (Note that the energy does not depend on k_y.) Hence we have that

$$\langle N + M - j, k_y, k_z | \hat{T}^{2B}(j, K_z; z) | N' + M' - j, k'_y, k'_z \rangle$$

$$\approx \langle 0, k_y, 0 | \hat{T}^{2B}(j = 0, K_z = 0; z = 0) | 0, k'_y, 0 \rangle$$

$$= \frac{-V_0}{L_y L_z} \phi^r_0(k_y l_r^2) \phi^r_0(k'_y l_r^2)$$

$$\times \left[1 + \frac{-V_0}{4\pi l_B^2 L_z} \sum_{N'', M'', k''_z} \frac{|B_0^{N''M''}|^2}{\varepsilon_{N'', k''_z} + \varepsilon_{M'', -k''_z}} \right]^{-1} .$$

$$\text{(A4)}$$

To extract an expression for the scattering length we put the above matrix element equal to the matrix element $\langle N + M - j, k_y, k_z | V_{pp} | N' + M' - j, k'_y, k'_z \rangle$ of the pseudopotential $V_{pp}(\mathbf{r}) = 4\pi a_{sc} \hbar^2 \delta(\mathbf{r}) / m$. From this we find that

$$\frac{m}{4\pi \hbar^2 a_{sc}} = -\frac{1}{V_0} + \frac{1}{4\pi l_B^2 L_z} \sum_{N, M, k_z} \frac{|B_0^{NM}|^2}{\varepsilon_{N, k_z} + \varepsilon_{M, -k_z}} . \quad \text{(A5)}$$

[1] P. Fulde and R. A. Ferrell, Phys. Rev. **135**, A550 (1964).

[2] A. I. Larkin and Yu. N. Ovchinnikov, Sov. Phys. JETP **20**, 762 (1965).

[3] H. A. Radovan, N. A. Fortune, T. P. Murphy, S. T. Hannahs, E. C. Palm, S. W. Tozer, and D. Hall, Nature (London) **425**, 51 (2003).

[4] K. Kakuyanagi, M. Saitoh, K. Kumagai, S. Takashima, M. Nohara, H. Takagi, and Y. Matsuda, Phys. Rev. Lett. **94**, 047602 (2005).

[5] M. W. Zwierlein, J. R. Abo-Shaeer, A. Schirotzek, C. H. Schunck, and W. Ketterle, Nature (London) **435**, 1047 (2005).

[6] M. W. Zwierlein, A. Schirotzek, C. H. Schunck, and W. Ketterle, Science **311**, 492 (2006).

[7] M. W. Zwierlein, C. H. Schunck, A. Schirotzek, and W. Ketterle, Nature (London) **442**, 54 (2006).

[8] G. B. Partridge, W. Li, R. I. Kamar, Y. A. Liao, and R. G. Hulet, Science **311**, 503 (2006).

[9] G. Sarma, J. Phys. Chem. Solids **24**, 1029 (1963).

[10] D. E. Sheehy and L. Radzihovsky, Phys. Rev. Lett. **96**, 060401 (2006).

[11] J. Kinnunen, L. M. Jensen, and P. Törmä, Phys. Rev. Lett. **96**, 110403 (2006).

[12] F. Chevy, Phys. Rev. Lett. **96**, 130401 (2006); e-print cond-mat/0605751.

[13] P. Pieri and G. C. Strinati, Phys. Rev. Lett. **96**, 150404 (2006).

[14] W. Yi and L.-M. Duan, Phys. Rev. A **73**, 031604(R) (2006).

[15] T. N. De Silva and E. J. Mueller, Phys. Rev. A **73**, 051602(R) (2006); Phys. Rev. Lett. **97**, 070402 (2006).

[16] M. Haque and H. T. C. Stoof, Phys. Rev. A **74**, 011602 (2006).

[17] T.-L. Ho and H. Zai, e-print cond-mat/0602568.

[18] A. Imambekov, C. J. Bolech, M. Lukin, and E. Demler, e-print cond-mat/0604423.

[19] K. Machida, T. Mizushima, and M. Ichioka, Phys. Rev. Lett. **97**, 120407 (2006).

[20] J.-P. Martikainen, Phys. Rev. A **74**, 013602 (2006).

[21] C.-C. Chien, Q. Chen, Y. He, and K. Levin, Phys. Rev. Lett. **97**, 090402 (2006); Phys. Rev. A **74**, 021602(R) (2006).

[22] M. M. Parish, F. M. Marchetti, A. Lamacraft, and B. D. Simons, e-print cond-mat/0605744.

[23] A. Bulgac and M. McNeil Forbes, e-print cond-mat/0606043.

[24] K. B. Gubbels, M. W. J. Romans, and H. T. C. Stoof, e-print cond-mat/0606330.

[25] W. C. Stwalley, Phys. Rev. Lett. **37**, 1628 (1976).

[26] E. Tiesinga, B. J. Verhaar, and H. T. C. Stoof, Phys. Rev. A **47**, 4114 (1993).

[27] D. M. Eagles, Phys. Rev. **186**, 456 (1969).

[28] A. J. Leggett, J. Phys. (Paris), Colloq. **41**, 7 (1980).

[29] P. Nozières and S. Schmitt-Rink, J. Low Temp. Phys. **59**, 195 (1985).

[30] See, for example, Evgeni Burovski, Nikolay Prokof'ev, Boris Svistunov, and Matthias Troyer, New J. Phys. **8**, 153 (2006).

[31] D. L. Feder, Phys. Rev. Lett. **93**, 200406 (2004).

[32] H. Shimahara and D. Rainer, J. Phys. Soc. Jpn. **66**, 3591 (1997).

[33] U. Klein, Phys. Rev. B **69**, 134518 (2004).

[34] K. Yang and A. H. MacDonald, Phys. Rev. B **70**, 094512 (2004).

[35] Q. Cui, C.-R. Hu, J. Y. T. Wei, and K. Yang, Phys. Rev. B **73**, 214514 (2006).

[36] A. M. Clogston, Phys. Rev. Lett. **9**, 266 (1962).

[37] A. H. MacDonald, H. Akera, and M. R. Norman, Phys. Rev. B **45**, 10147 (1992).

[38] See, for example, J. R. Schrieffer, *Theory of Superconductivity* (Westview Press, Boulder, 1999).

[39] H. T. C. Stoof, M. Bijlsma, and M. Houbiers, J. Res. Natl. Inst. Stand. Technol. **101**, 443 (1996).

[40] H. Akera, A. H. MacDonald, S. M. Girvin, and M. R. Norman, Phys. Rev. Lett. **67**, 2375 (1991); M. R. Norman, A. H. MacDonald, and H. Akera, Phys. Rev. B **51**, 5927 (1995).

[41] L. P. Gorkov and T. K. Melik-Barkhudarov, Sov. Phys. JETP **13**, 1018 (1961).

[42] M. Marinescu and L. You, Phys. Rev. Lett. **81**, 4596 (1998).

[43] M. Baranov, L. Dobrek, K. Gorall, L. Santos, and M. Lewenstein, Phys. Scr. **T102**, 74 (2002).

[44] V. Schweikhard, I. Coddington, P. Engels, V. P. Mogendorff, and E. A. Cornell, Phys. Rev. Lett. **92**, 040404 (2004).

[45] N. Regnault and T. Jolicoeur, Phys. Rev. B **70**, 241307(R) (2004).